### Title

Reservoir Water-Quality Projections under Climate-Change Conditions




### Journal

Water Resources Management, 33(1)

### ISSN

0920-4741



### Authors

Azadi, Firoozeh

Ashofteh, Parisa-Sadat

Loáiciga, Hugo A



### Publication Date

2019

### DOI

10.1007/s11269-018-2109-z

Peer reviewed

Water Resources Management (2019) 33:401–421
https://doi.org/10.1007/s11269-018-2109-z

# Reservoir Water-Quality Projections under Climate-Change Conditions

Firoozeh Azadi[1] · Parisa-Sadat Ashofteh[1] · Hugo A. Loáiciga[2]

Received: 7 May 2018 / Accepted: 16 September 2018 /
Published online: 26 September 2018


## Abstract

Reservoirs are key components of water infrastructure that serve many functions (water supply, hydropower generation, flood control, recreation, ecosystem services, etc.). Climate change affects the hydrology of the tributary areas to reservoirs, which may profoundly impact their operation and possibly the reservoirs' water quality, among which the temperature gradient and the total dissolved solids (TDS) are key qualitative characteristics of reservoirs, especially those with irrigation function. This study examines water-quality changes in the Aidoghmoush reservoir (East Azerbaijan-Iran) under climate-change conditions in the period 2026–2039. The temperature and precipitation climate variables are calculated by the HadCM3 model driven by emission scenario A2 in the baseline period (1987–2000), and these variables are then projected over the future period (2026–2039). The average annual runoff under climate-change conditions is simulated by the IHACRES model. The results show the future average annual runoff would decrease by about 1% compared to the baseline conditions. The CE-QUAL-W2 model is employed to simulate the reservoir water quality. It is predicted the surface air temperature would increase by 1.3 °C under the climate-change scenario compared to the baseline condition, and the temperatures of the reservoir's surface- and bottom-waters would increase by 1.19 and 1.24 °C, respectively. The average TDS near the reservoir surface would increase by 44.5 g/m$^3$ (4.3%) relative to baseline TDS. The TDS near the reservoir surface are projected to be highest in autumn and winter for baseline and future conditions. This research shows that changes due to climate change are potentially severe, and presents a methodology that could assist managers and planners to find optimal strategies of reservoir operation to cope with changes in thermal stratification and TDS. This paper results identify the reservoir levels from which to withdraw water with the best water-quality characteristics.

**Keywords** Reservoirs · Water quality · Climate change · CE-QUAL-W2 model · TDS concentration

✉ Parisa-Sadat Ashofteh
ps.ashofteh@qom.ac.ir

Extended author information available on the last page of the article

## 1 Introduction

The velocity of streamflow declines upon entering a reservoir. This causes thermal stratification due to the variation in the density of water with depth as a result of uneven mixing. Reservoirs modify the water quality of incoming streamflow. Such changes may be deleterious to downstream riverine ecosystems. Therefore, prediction of water-quality changes and associated water withdrawal policies under climate change are essential. Several pertinent publications about water quality in reservoirs are reviewed below.

Debele et al. (2008) integrated hydrological and water-quality models (SWAT and CE-QUAL-W2) to simulate the combined processes of water quantity and quality in the Cedar Creek Reservoir, Texas (United States). Liu et al. (2009) investigated the impact of phosphorus load reduction on water quality in a stratified eutrophicated reservoir employing the CE-QUAL-W2 model. Chung and Gu (2009) assessed the fate and transport processes of the herbicide atrazine in the Saylorville Reservoir, Iowa. The CE-QUAL-W2 was incorporated with a sub-model for toxic contaminants. Lee et al. (2012) reported the effect of climate change on the thermal structure of lakes in response to watershed hydrology. They applied a hydrodynamic water quality model coupled to a hydrological model with a future climate scenario projected with general circulation model (GCM) driven by the A2 greenhouse gasses emission scenario to the Yongdam Reservoir (South Korea). Liu and Chen (2013) presented the modeling of hydrothermal characteristics and suspended solids in the Shihmen Reservoir in northern Taiwan. The model was validated with measured data of water surface elevation, water temperature, and concentration of suspended solids. Shokri et al. (2014) investigated crisis management due to the sudden entrance of a 30 $m^3$ methyl tert-butyl ether (MTBE) load to the Karaj dam in Iran. Simulation of MTBE advection, dispersion, and vaporization were added to the CE-QUAL-W2 model. The multi-objective NSGAII-ALANN algorithm was employed to calculate the best set of decisions in which the two aforementioned damages were minimized. Butcher et al. (2015) estimated the sensitivity of lake thermal and mixing dynamics to climate change in 27 lake "archetypes" representative of a range of lakes and reservoirs occurring throughout the United States. Peng et al. (2016) reported numerical simulations and influencing factors of seasonal manganese pollution in reservoirs. They presented a reservoir manganese pollution model by adding a manganese biogeochemical module to CE-QUAL-W2. The model was applied to the Wangjuan reservoir (Qingdao, China). Amirkhani et al. (2016) presented an approach for the optimal operation of a Karaj reservoir in Iran with two objectives: (Amirkhani et al., 2016) the minimization of TDS in reservoir releases, and (Ashofteh et al., 2013) the minimization of the temperature difference between inflow to the reservoir and released water from the reservoir. The CE-QUAL-W2 model was coupled with the nondominated sorting genetic algorithm-II (NSGA-II) to produce a simulation-optimization method under four scenarios (seasons). Soleimani et al. (2016) reported a methodology for extracting optimal operational rules for selective reservoir water withdrawal by considering fixed levels of Karkheh reservoir (Iran) water outlets for thermal control. A data-mining model (the LIBSVM model) was applied as a surrogate model of the CE-QUAL-W2 model and coupled with a genetic algorithm (GA), resulting in the LIBSVM-GA algorithm. The selective withdrawal approach considered four fixed reservoir outlets, located at 120, 140, 163, and 181 m above sea level, to account for reservoir thermal stratification. Yazdi and Moridi (2017) developed an integrated model for simulating and evaluating the water quality protection strategies of reservoirs. The Soil and Water Assessment Tool (SWAT) model was applied for modeling of the surface runoff and transportation of pollutant load over

the watershed area. The CE-Qual-W2 was implemented for simulating the reservoir water quality. These models were linked to simulate the transmission and distribution of water quality variables in the Seimare watershed-reservoir system (Iran). Heidarzadeh and Motiey Nejad (2017) simulated the TDS with CE-QUAL-W2 under two scenarios corresponding to "with" and "without" sedimentation in normal, dry, and wet periods of inflow to the Shahriyar reservoir, Iran. The calculated TDS posed no limitation to agricultural water based on the FAO's irrigation guidelines. Vaighan et al. (2017) addressed the separate and combined impacts of climate and land use change on streamflow, suspended sediment, and water quality in the Kor River Basin, (Iran) with the BASINS–WinHSPF model. The calibrated model was run under two climate changes, two land use changes and four combined change scenarios for 2020–2049. Sabeti et al. (2017) studied thermal regime and salinity in the Mamloo Dam in Tehran province (Iran) implementing the CE-QUAL-W2 model to simulate the thermal regime and salinity through 2020.

This paper's novel contribution is assessment of changes in TDS driven by climate change conditions, a topic not yet reported in previous studies. Most previous researches have focused on other water characteristics under climate change, or have considered TDS without accounting for climate change. The assessment of TDS dynamics under climate change appears novel. Furthermore, this work addresses the effect of changes in surface-air temperature on TDS, and thermal stratification, which has not been reported in the published literature. The effect of temperature and other climatic parameters on the concentration of water constituents (TDS) and the effect of TDS on the water temperature profile under climate change are successfully resolved in this work.

This paper establishes that climate change may affect the quantity and quality of water resources, and shows that optimal operation of reservoirs would be necessary to adapt to changing climatic conditions. This paper demonstrates the methodology herein introduced to predict water quality characteristics under climatic change and associated adaptive optimal reservoir operation with one important reservoir in Iran (the Aidoghmoush reservoir, East Azerbaijan), whose downstream network one of the most productive agricultural regions in the country (with a area under cultivation of about 13,500 ha of agricultural crops).

## 2 Methodology

This paper's methodology includes climatic simulation and calculation of reservoir inflow coupled with the implementation of the CE-QUAL-W2 model for reservoir water-quality simulation. The flowchart of this paper's methodology is shown in Fig. 1.

### 2.1 Case Study

The study basin is the Aidoghmoush basin with an area of approximately 1802 $km^2$ located in East Azerbaijan province, Iran (Fig. 2). The river is 80 km long and flows into the Ghezel Ozan River (Ashofteh et al., 2013). The present study concerns the Aidoghmoush Dam and reservoir located on the Aidoghmoush River, which has an intake tower and a bottom outlet. Four valves are located in the intake tower. The components of Aidoghmoush dam include the body of the dam, weir, water diversion system (capacity of 310 $m^3/s$), and the intake system and bottom outlet. The intake for agricultural water is through a tower (with a discharge capacity of 14.7 $m^3/s$), which has four intake valves at elevations of 1306, 1318, 1326, and 1333 m above sea level. The bottom outlet valve is located at an elevation of 1319.55 m above

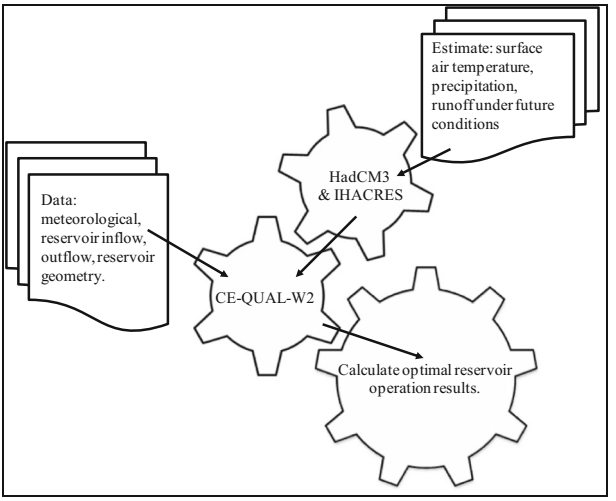


**Fig. 1** Flowchart of paper's methodology

sea level, which has a discharge capacity 55 $m^3/s$. The crown length of the dam and its height from the foundation equal 297 m and 67 m, respectively. Also, the normal volume of the reservoir is $145.7 \times 10^6$ $m^3$. The normal water level and the maximum flood level equal 1341.5 and 1348.3 m above sea level, respectively.

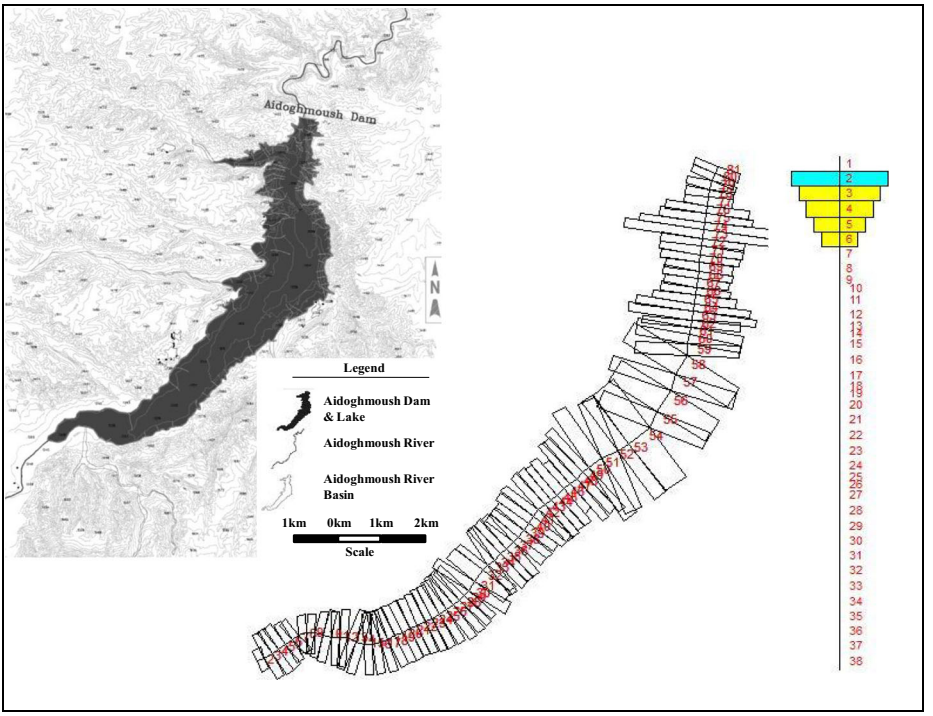


**Fig. 2** Outline and geometry modeled in the CE-QUAL-W2. There are 81 2-D (plan) sections and 38 depth layers

The TDS is a key water-quality characteristic in many Iranian rivers due to its arid climate. Input of drainage water, water flow from soil layers with high dissolution and high evaporation rates are the main reasons for the relatively high suspended solids in Iran's freshwater. For this reason TDS was selected as a water quality indicator under climate change in the Aidoghmoush reservoir, whose downstream irrigation network is one of the most productive agricultural regions in Iran.

The raw data used in the present study include meteorological and hydrological observed data from the Meteorological Organization (Ministry of Power, Iran) and the Regional Water Organization of East Azerbaijan (Iran), respectively. Simulations of air temperature and rainfall for the baseline and climate change periods were extracted from the IPCC website (IPCC-DDC, 1988). Reservoir inflow and water demand during the climate change period were reported by Ashofteh et al. (2017a).

### 2.2 Climate Preprocessing and Estimation of the Volume of Water Resources and Water Uses under Climate-Change Conditions

The period 1987–2000 serves as the baseline period as recommended by the Intergovernmental Panel on Climate Change (IPCC-TGCIA, 1999), the period 2026–2039 is the future period for projections of water quality. The HadCM3 model was employed for projecting climate variables corresponding to the A2 emission scenario (IPCC-DDC, 1988). The climate projections were reported by Ashofteh et al. (2017a). Those projections show the temperature in the future period would increase by 1.3 °C compared to the baseline period. The downscaled climatic data were input to the IHACRES model to simulate future runoff. The runoff simulations are found in Ashofteh et al. (2017b). The projected reservoir inflow in the future period would decrease 1% compared to the baseline period, while the volume of irrigation water demand would increase by 16% (Ashofteh et al., 2017a).

### 2.3 Water-Quality Simulation with the CE-QUAL-W2 Model

The CE-QUAL-W2 3.7 model (Cole and Wells, 2006) is widely used to simulate water quality in reservoirs and rivers. It was herein adopted to simulate quality parameters in the Aidogmoush Dam reservoir. The model is 2-dimensional (longitudinal and vertical) and averaged over the width. It is written in FORTRAN language. The reservoir was simulated with 81 sections and 38 depth layers respectively (see Fig. 2). CE-QUAL-W2 simulations require geometric data, meteorological data, initial conditions (temperature and depth of water on the first simulation day), and boundary conditions (reservoir inflow and outflow data, and reservoir inflow water temperature). The topography and geometry of the reservoir modeled in the software on the plan and depth are shown in Fig. 2. The main equations governing the CE-QUAL-W2 model, including the hydrodynamic flow equations (continuity and momentum equations), and the advection-dispersion equations, are presented in Table 1. Figure 3 depicts the flowchart of the reservoir water-quality modeling.

The projection of future water quality in the Aidoghmoush reservoir would indicate the best levels to withdraw water from for downstream use. Water temperature affects TDS distribution in the reservoir. Variations in water temperature cause a change in the density of water with ensuing thermal stratification. Three thermal stratifications, namely, the Epilimnion, Metalimnion and Hypolimnion are observed in the Aidoghmoush reservoir. Figure 4 shows a schematic of thermal stratification, changes in oxygen, and TDS with water depth in the

**Table 1** Main equations governing the ***CE-QUAL-W2*** model

| Type | Equation |
|---|---|
| Horizontal momentum equation | $\frac{\partial UB}{\partial t}+\frac{\partial UUB}{\partial x}+\frac{\partial WUB}{\partial z}=gB\sin\alpha+g\cos\alpha B\frac{\partial\eta}{\partial x}-\frac{g\cos\alpha B}{\rho}\int_{\eta}^{z}\frac{\partial\rho}{\partial x}dz+\frac{1}{\rho}\frac{\partial B\tau_{xx}}{\partial x}+\frac{1}{\rho}\frac{\partial B\tau_{xz}}{\partial z}+qBU_x$ |
| Vertical momentum equation | $0=g\cos\alpha-\frac{1}{\rho}\frac{\partial p}{\partial z}$ |
| Continuity equation | $\frac{\partial UB}{\partial x}+\frac{\partial WB}{\partial Z}=qB$ |
| State equation | $\rho=F(T_W,\Phi_{TDS},\Phi_{SS})$ |
| Free surface equation | $B_\eta\frac{\partial\eta}{\partial t}=\frac{\partial}{\partial x}\int_{\eta}^{h}UBdz-\int_{\eta}^{h}qBdz$ |
| Water quality transport equation | $\frac{\partial B\Phi}{\partial t}+\frac{\partial UB\Phi}{\partial x}+\frac{\partial WB\Phi}{\partial z}-\frac{\partial\left(BD_x\frac{\partial\Phi}{\partial x}\right)}{\partial x}-\frac{\partial\left(BD_z\frac{\partial\Phi}{\partial z}\right)}{\partial z}=q_\Phi B+s_\Phi B$ |

in which, $\eta$ = water level (m); $W$ and $U$ = the mean velocity in the longitudinal and vertical directions, respectively (m/s); $B$ = control volume width; $\tau$ = tensions at the $xx$ and $xz$ surfaces (N/m$^2$ ); $\alpha$ = slope; $q$ = inflow to control volume (m$^3$ /s); $TW$ = water temperature (°C); $\Phi$ = the concentration of pollutants (in here, TDS); $D_x$ and $D_z$ = the diffusion coefficient of heat and pollution in the directions of the longitudinal and vertical, respectively; $q_\Phi$ = inflow or outflow; $B_\Phi$ = width at the surface (m); and $s_\Phi$ = input or output pollution by other sources (m$^3$ /s)

reservoir. Figure 4 depicts the depth profile corresponding to complete thermal stratification, complete mixing, and reverse thermal stratification, water density, and TDS variation.

## 3 Results and Discussion

The geometry of the reservoir was modeled in the CE-QUAL-W2 software. The required data for simulating reservoir water quality were input to input to CE-QUAL-W2. The geometry of the reservoir was calibrated with a coefficient of determination equal to 99.7%.

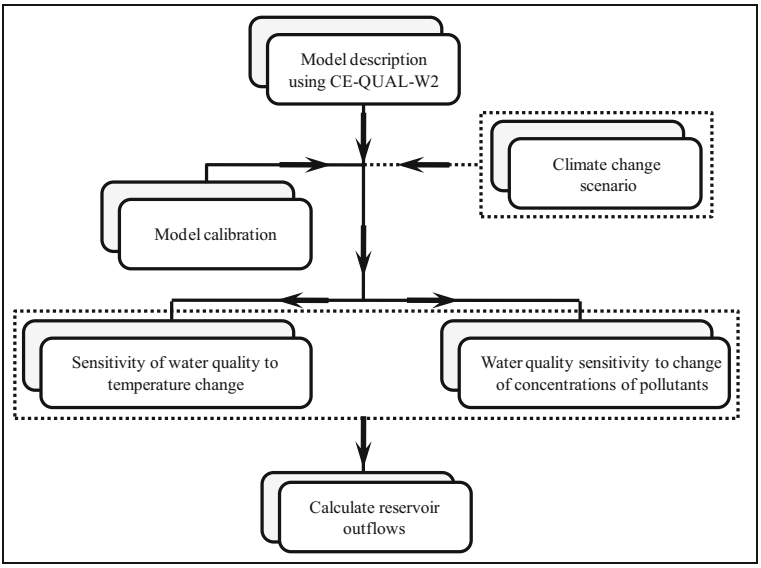


**Fig. 3** Flowchart of the reservoir water-quality modeling

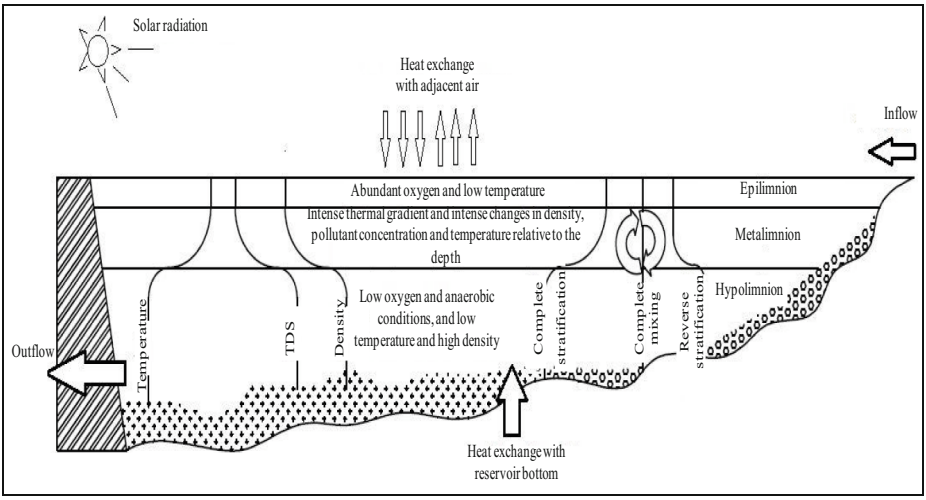


**Fig. 4** Generic diagram of water-quality stratification in a reservoir

### 3.1 Comparison of TDS under Baseline and Climate-Change Periods in the reservoir's Surface and Bottom Waters

Figure 5 and Tables 2 and 3 depict comparisons of the simulated TDS variations in reservoir surface water during the simulation period for climate-change conditions relative to the baseline period. The results demonstrate that during the 14-year simulation period for climate change conditions the maximum TDS available at the water surface would occur in January 2038 and it would equal 1980 g/m$^3$. During the 14-year simulation for the baseline period maximum TDS of the surface water occurred on ebruary 15th, 2000, equaling 1616 g/m$^3$. The average TDS concentration of water during the 14-year simulation period under climate-change conditions would be higher than the average during the baseline period, which would equal 1075 and 1031 g/m$^3$, respectively. Simulation results show TDS concentration of surface water under baseline and climate-change conditions would peak in the autumn and winter seasons for every year of the 14-year simulation periods. It follows from comparing the magnitude and timing of the annual maximum concentrations in surface water for the corresponding years that in 10 years of the 14-

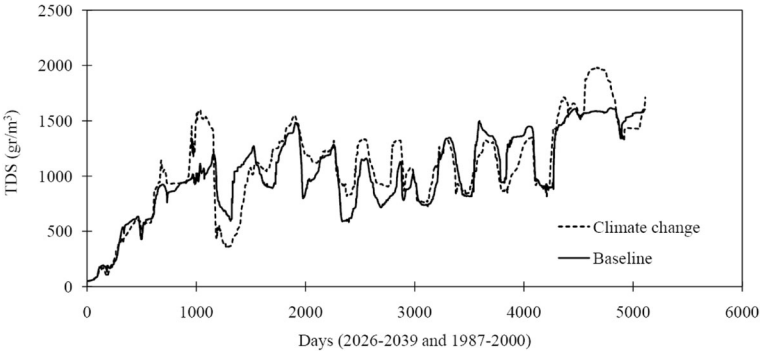


**Fig. 5** Comparison of the TDS in reservoir surface water during the climate change period compared the TDS during the baseline period

**Table 2** The concentration and timing of maximum TDS on the water surface

| Base period | | | | Climate-change period | | | |
|---|---|---|---|---|---|---|---|
| Year | maximum TDS ($g/m^3$) | Julian day | Day-month | Year | maximum TDS ($g/m^3$) | Julian day | Day-month |
| 1987 | 562 | 365 | 31-Dec | 2026 | 473 | 365 | 31-Dec |
| 1988 | 923 | 691 | 21-Dec | 2027 | 1141 | 678 | 9-Nov |
| 1989 | 1113 | 1035 | 31-Oct | 2028 | 1598 | 1036 | 1-Nov |
| 1990 | 1200 | 1158 | 3-Mar | 2029 | 1523 | 1098 | 2-Jan |
| 1991 | 1360 | 1826 | 31-Dec | 2030 | 1437 | 1826 | 31-Dec |
| 1992 | 1484 | 1908 | 22-Mar | 2031 | 1549 | 1893 | 8-Mar |
| 1993 | 1284 | 2258 | 7-Mar | 2032 | 1340 | 2522 | 26-Nov |
| 1994 | 1158 | 2558 | 1-Jan | 2033 | 1323 | 2867 | 6-Nov |
| 1995 | 1337 | 3287 | 31-Dec | 2034 | 1313 | 3287 | 31-Dec |
| 1996 | 1499 | 3594 | 2-Nov | 2035 | 1325 | 3647 | 26-Dec |
| 1997 | 1425 | 4018 | 31-Dec | 2036 | 1322 | 3653 | 1-Jan |
| 1998 | 1530 | 4383 | 31-Dec | 2037 | 1713 | 4365 | 13-Dec |
| 1999 | 1608 | 4470 | 28-Dec | 2038 | 1981 | 4669 | 13-Oct |
| 2000 | 1617 | 4794 | 15-Feb | 2039 | 1945 | 4749 | 1-Jan |

year simulation periods the maximum annual TDS concentration in surface water under climate-change conditions would exceed that under the baseline period, and it would be less in 4 years than that of the baseline period. Moreover, the time of peak annual concentration in surface water would occur earlier in 6 years of the 14 year-simulation period under climate-change conditions compared with the time of occurrence under baseline conditions, it would occur at the same time in 4 years, and it would occur later than the baseline condition in 4 years. Simulation results for the minimum TDS in surface water indicate the minimum TDS over the entire 14-year simulation period would occur in winter in the first 3 years of the period under climate-change conditions, and it would occur in winter and spring under baseline conditions. During the rest of the simulation period under baseline and climate-change conditions would occur in the spring and summer seasons (except for 2033, which exhibits autumnal occurrence). Also, comparison of the

**Table 3** The concentration and timing of minimum TDS on the water surface

| Base period | | | | Climate change period | | | |
|---|---|---|---|---|---|---|---|
| Year | minimum TDS ($g/m^3$) | Julian day | Day-month | Year | minimum TDS ($g/m^3$) | Julian day | Day-month |
| 1987 | 51 | 1–5 | 1–5, Jan | 2026 | 51 | 1–5 | 1–5, Jan |
| 1988 | 425 | 498 | 12-May | 2027 | 475 | 366 | 1-Jan |
| 1989 | 760 | 732 | 1-Jan | 2028 | 927 | 750 | 20-Jan |
| 1990 | 592 | 1313 | 5-Aug | 2029 | 346 | 1283 | 6-Jul |
| 1991 | 889 | 1697 | 24-Aug | 2030 | 929 | 1462 | 1-Jan |
| 1992 | 796 | 1978 | 31-May | 2031 | 1122 | 2091 | 22-Sep |
| 1993 | 582 | 2397 | 24-Jul | 2032 | 818 | 2378 | 5-Jul |
| 1994 | 715 | 2691 | 14-May | 2033 | 866 | 2901 | 10-Sep |
| 1995 | 724 | 3120 | 17-Jul | 2034 | 761 | 3086 | 13-Jun |
| 1996 | 814 | 3520 | 20-Aug | 2035 | 826 | 3472 | 4-Jul |
| 1997 | 937 | 3822 | 18-Jun | 2036 | 844 | 3851 | 17-Jul |
| 1998 | 850 | 4201 | 2-Jul | 2037 | 815 | 4209 | 10-Jul |
| 1999 | 1515 | 4517 | 14-May | 2038 | 1519 | 4523 | 20-May |
| 2000 | 1341 | 4887 | 18-May | 2039 | 1319 | 4912 | 13-Jun |

duration of the minimum annual TDS concentration in surface water during the 14-year simulation period shows that over 7 years the minimum annual TDS concentration in surface water under climate-change conditions would have a shorter duration than under baseline conditions. Furthermore, the minimum TDS would occur earlier under climate-change conditions than under baseline conditions in 6 years, and it would occur at the same time in 1 year.

Figure 6 and Tables 4 and 5 show comparisons of the TDS variations in reservoir bottom water during the simulation period under climate-change conditions relative to the baseline period. The results show during the 14-year simulation periods for the climate-change and baseline periods the maximum TDS in the reservoir's bottom water would occur on January 5th, 2039, and occurred on December 19th, 2000, with respective magnitudes equal to 1927 and 1616 g/m$^3$. The average TDS concentration of the reservoir bottom water during the 14-year simulation period for climate-change conditions would be higher than that of the baseline period, with the respective concentrations equaling 1232 and 1227 g/m$^3$ for climate change and baseline conditions. Also, the simulation results show TDS of the reservoir bottom water corresponding to the baseline and climate-change periods would peak in the autumn and winter seasons every year of the 14-year simulation period (except in years 2031, 2037, and 1992 when there is summer occurrence). Comparing the magnitude and timing of the annual maximum concentrations in the reservoir bottom water, it was projected that in 7 years of the 14-year simulation periods the maximum annual TDS concentration in reservoir bottom water under climate-change conditions exceeds the baseline concentration, and it would be less than the baseline concentration in the other 7 years. Moreover, the time of the peak annual concentration in reservoir bottom water in 10 of the 14-years of simulation under climate-change conditions would occur earlier than during the base conditions, and it would occur later than during the baseline period in 4 years. Simulation results for the minimum TDS of the reservoir bottom water indicate minimum TDS over the entire 14-year simulation periods for climate-change and baseline conditions would occur in autumn and winter. Also, comparison of the timing of the minimum annual TDS concentration in reservoir bottom water during the 14-year simulation periods shows that in 4 years the minimum annual TDS concentration in reservoir bottom water under climate-change conditions would occur later than during the baseline period, it would occur earlier in 3 years, and it would occur at the same time in 7 years.

### 3.2 Calculated Temperature Gradient with and without TDS

Figure 7 depicts the temperature profile over the reservoir's depth with and without TDS during the climate-change period at the beginning (2026), middle (2032), and end of the

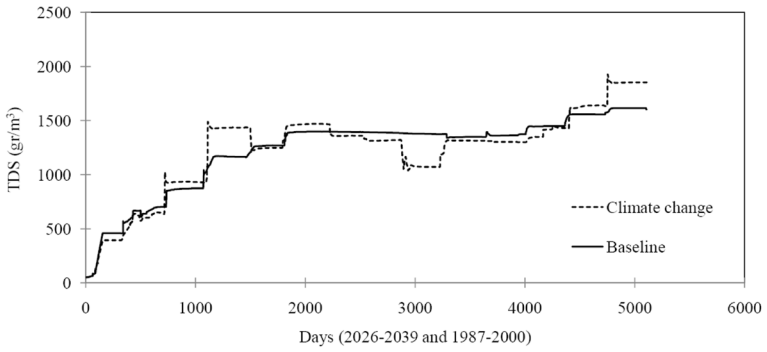


**Fig. 6** Comparison of TDS in reservoir bottom water during the climate-change period compared to the baseline period

**Table 4** The concentration and timing of maximum TDS on the bottom of the reservoir

| Base period | | | | Climate change period | | | |
|---|---|---|---|---|---|---|---|
| Year | maximum TDS ($g/m^3$) | Julian day | Day-month | Year | maximum TDS ($g/m^3$) | Julian day | Day-month |
| 1987 | 570 | 340 | 6-Dec | 2026 | 473 | 365 | 31-Dec |
| 1988 | 703 | 731 | 31-Dec | 2027 | 1024 | 720 | 21-Dec |
| 1989 | 1042 | 1074 | 9-Dec | 2028 | 939 | 1096 | 31-Dec |
| 1990 | 1171 | 1184 | 29-Mar | 2029 | 1489 | 1112 | 16-Jan |
| 1991 | 137 | 1825 | 30-Dec | 2030 | 1437 | 1826 | 31-Dec |
| 1992 | 1400 | 2071 | 1-Sep | 2031 | 1472 | 2050 | 12-Aug |
| 1993 | 1399 | 2195 | 3-Jan | 2032 | 1468 | 2192 | 1-Jan |
| 1994 | 1392 | 2570 | 13-Jan | 2033 | 1324 | 2558 | 1-Jan |
| 1995 | 1382 | 2923 | 1-Jan | 2034 | 1313 | 3287 | 31-Dec |
| 1996 | 1395 | 3651 | 29-Dec | 2035 | 1319 | 3296 | 9-Jan |
| 1997 | 1425 | 4018 | 31-Dec | 2036 | 1311 | 3689 | 6-Feb |
| 1998 | 1529 | 4383 | 31-Dec | 2037 | 1447 | 4254 | 24-Aug |
| 1999 | 1577 | 4748 | 31-Dec | 2038 | 1641 | 4717 | 30-Nov |
| 2000 | 1617 | 5102 | 19-Dec | 2039 | 1927 | 4753 | 5-Jan |

simulation period (2039). Figure 7 (a) indicates the temperature in the presence of TDS would decrease by 0.003 °C in the winter of 2026 relative to the temperature without TDS in the same year, and the temperature profiles are nearly identical to each other. The simulated temperature profile in year 2032 [Fig. 7(b)] indicates the temperature profile in the absence of TDS is almost uniform, but it varies with depth in the presence of TDS, and there is a clear stratification. Furthermore, the thermal difference with and without TDS is about 2 °C, and the stratification is reversed with depth. At the end of the simulation period (2039) [Fig. 7 (c)] the water temperature with TDS would be less than the temperature without TDS. In the spring (Figures (d), (e), (f)) and summer [Figures (g), (h), (i)], the temperature profiles with and without TDS are similar with small discrepancies between them. In the autumn, [Figures (j), (k), (l)] the temperature profiles are similar but the temperature without TDS is the lower of the

**Table 5** The concentration and timing of minimum TDS on the bottom of the reservoir

| Base period | | | | Climate change period | | | |
|---|---|---|---|---|---|---|---|
| Year | minimum TDS ($g/m^3$) | Julian day | Day-month | Year | minimum TDS ($g/m^3$) | Julian day | Day-month |
| 1987 | 51 | 1–4 | 1–4, Jan | 2026 | 51 | 1–4 | 1–4, Jan |
| 1988 | 564 | 366 | 1-Jan | 2027 | 475 | 366 | 1-Jan |
| 1989 | 760 | 732 | 1-Jan | 2028 | 922 | 1079 | 14-Dec |
| 1990 | 1029 | 1097 | 1-Jan | 2029 | 941 | 1097 | 1-Jan |
| 1991 | 1161 | 1462 | 1-Jan | 2030 | 1224 | 1530 | 10-Mar |
| 1992 | 1360 | 1827 | 1-Jan | 2031 | 1438 | 1827 | 1-Jan |
| 1993 | 1392 | 2557 | 31-Dec | 2032 | 1325 | 2557 | 31-Dec |
| 1994 | 1382 | 2922 | 31-Dec | 2033 | 1053 | 2894 | 3-Dec |
| 1995 | 1350 | 3287 | 31-Dec | 2034 | 1038 | 2935 | 13-Jan |
| 1996 | 1340 | 3290 | 3-Jan | 2035 | 1310 | 3652 | 31-Dec |
| 1997 | 1361 | 3709–3711 | 25–27, Feb | 2036 | 1300 | 3708 | 25-Feb |
| 1998 | 1427 | 4019 | 1-Jan | 2037 | 1311 | 4019 | 1-Jan |
| 1999 | 1530 | 4384 | 1-Jan | 2038 | 1430 | 4398 | 15-Jan |
| 2000 | 1577 | 4749 | 1-Jan | 2039 | 1633 | 4749 | 1-Jan |

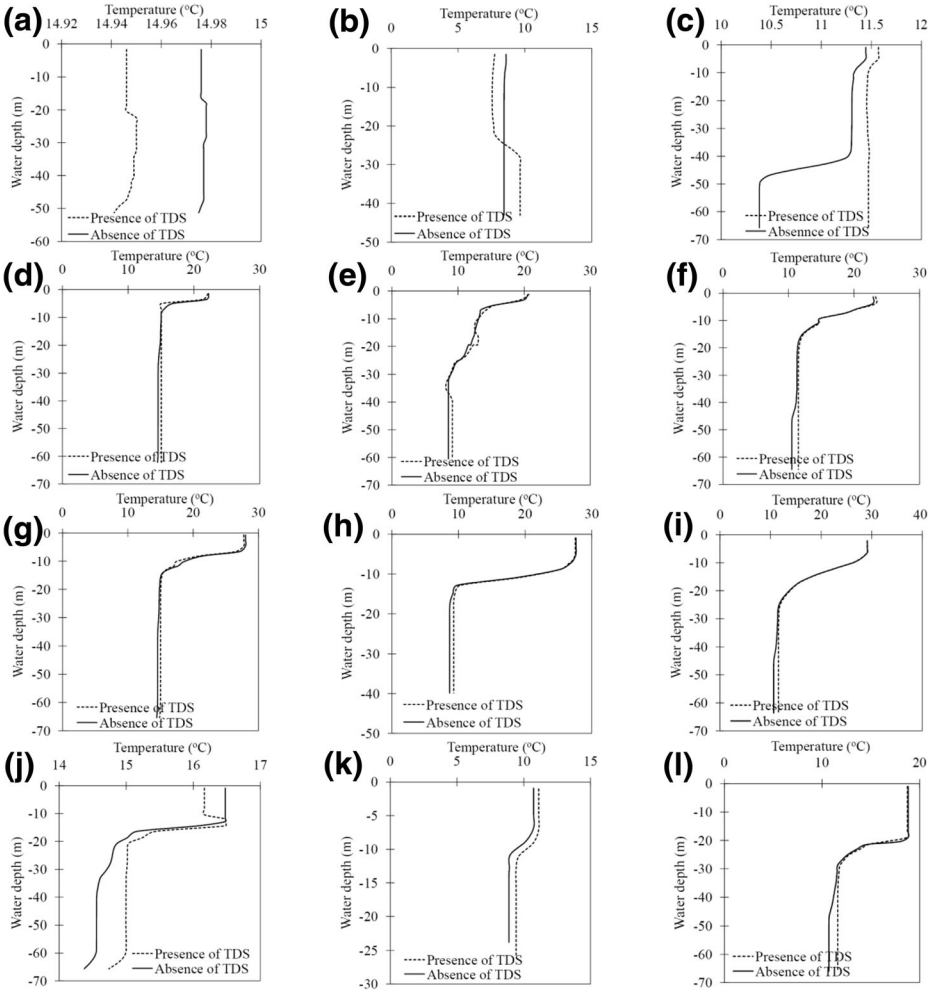


**Fig. 7** Comparison of the simulated temperature profile over the reservoir's depth with and without TDS under climate-change conditions in the middle of the winter (a) at the beginning of 2026, (b) mid 2032, and (c) end of 2039; in the middle of the spring (d) at the beginning of 2026, (e) mid 2032, and (f) end of 2039; in the middle of the summer (g) at the beginning of 2026, (h) mid 2032, and (i) end of 2039; and in the middle of the autumn (j) at the beginning of 2026, (k) mid 2032, and (l) end of 2039

two, with the temperature differential increasing with increasing depth. These results indicated the effect of TDS on thermal stratification and temperature is more pronounced in the cold season compared with the warm season.

### 3.3 TDS Variation with Reservoir Depth under Climate-Change Conditions

Figures 8 and 9 depict the TDS profiles under climate-change conditions relative to the baseline period in the middle of the two simulation periods in mid winter, mid spring, mid summer, and mid autumn. The middle years of the baseline and climate-change periods are 1993 (Fig. 8) and 2032 (Fig. 9), respectively, and the middle of each season corresponds to the middle day of the middle month.

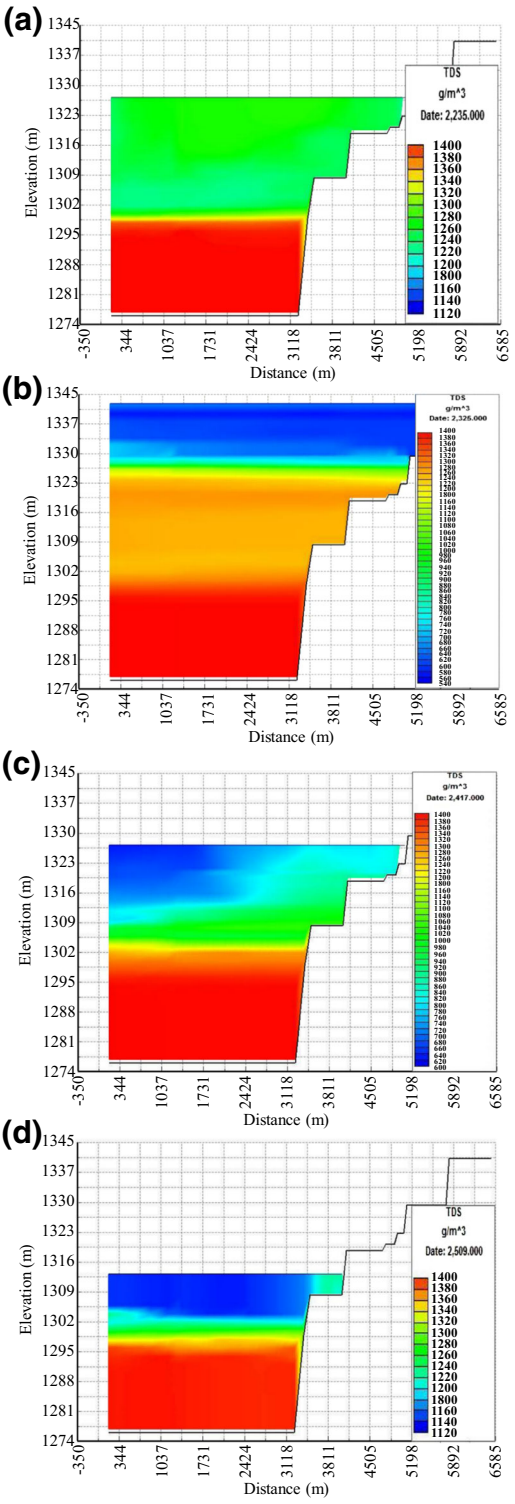


**Fig. 8** Comparison of TDS profiles with respect to distance along the reservoir from the dam over the reservoir's depth in 1993 in the middle of the (a) winter; (b) spring; (c) summer; and (d) autumn

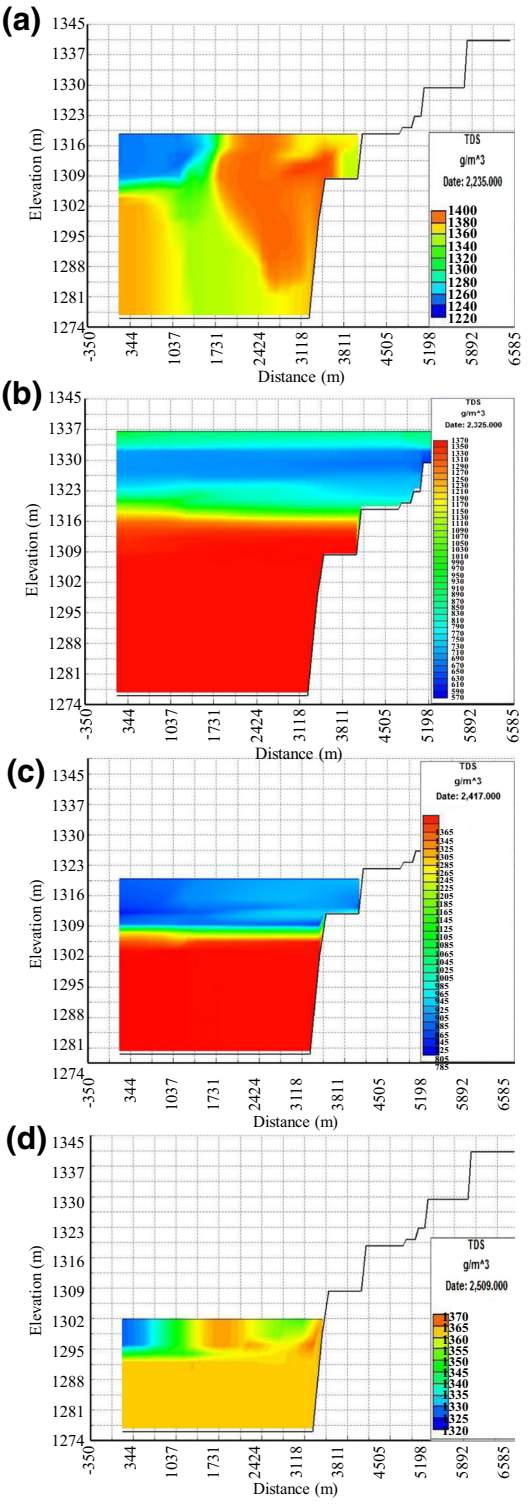


**Fig. 9** Comparison of TDS profiles with respect to distance along the reservoir from the dam over the reservoir's depth in 2032 in the middle of the (a) winter; (b) spring; (c) summer; and (d) autumn

It is seen in Fig. 8 (a) there is a pronounced variation of TDS with depth in winter for the baseline period within the Metalimnion. The thickness of this stratification is about 7 m (1,295 to 1302 m above sea level). The TDS increases with depth due to the low temperature and high water density, and the TDS decreases on the water surface. The TDS at a depth of 1380 m above sea level is about 1260 g/m$^3$. Figure 9 (a) depicts the TDS profile in winter under climate-change conditions. In deep areas the TDS concentration is relatively high. The TDS profile is very different relative to the baseline period, and the TDS varies along the length of the reservoir. The highest TDS near the dam is from the water surface to a height of about 1281 m (about 35 m thick layer). Concentrations are high in this region. The maximum and minimum TDS equal respectively 1390 and 1230 g/m$^3$. A minimum TDS is observed near the dam, and the TDS increases with increasing depth, while the TDS on the water surface increases with decreasing distance from the dam. This may be due to changes in reservoir inflow and air temperature under climate-change conditions.

Figure 8 (b) portrays the trend of TDS changes under baseline conditions in the spring. It is seen in Fig. 8 (b) several areas in the reservoir have a high TDS variation. These areas are located at heights varying between 1295 and 1302, from 1323 to 1330, and from 1337 to 1343 m above sea level. The TDS at maximum depth reach about 1400 g/m$^3$ and decrease towards the water surface. Figure 9 (b) shows the variations of TDS with depth under climate-change conditions in the spring. It is seen in Fig. 9 (b) a pronounced TDS variation (between 1312 and 1337 m above sea level). In this region the TDS vary from 1350 g/m$^3$ to 850 g/m$^3$ (at near the surface of the water). The concentration at depth reaches 1370 g/m$^3$.

Figure 8 (c) displays the TDS profile in the reservoir for baseline conditions in the summer. Pronounced variation in TDS can be seen from the water surface to a large depth (about 30 m). In this region TDS vary between 660 and 1380 g/ m$^3$. In the areas near the Aidoghmoush reservoir entrance (most distant from the dam) the TDS are low and increases towards the central areas. Figure 9 (c) depicts projected changes in TDS under climate-change conditions in the summer. The TDS vary from 1345 g/m$^3$ (at a height of 1300 m) to 825 g/m$^3$. The concentration increases with depth to about 1365 g/m$^3$. TDS changes would be significant in a region where large temperature changes are likely to occur. The thickness of this area is about 14 m.

Figure 8 (d) depicts the variation TDS in autumn corresponding to the baseline period. The TDS near the entrance of the reservoir are about 1160 g/m$^3$, and the TDS increase towards the central area of the reservoir. Also, the TDS increases with increasing depth. The TDS changes are distinctly pronounced in the Metalimnion. The TDS vary in this area from 1380 to 1129 g/ m$^3$. The region is between 1295 to about 1306 m above sea level. TDS in bottom water near the dam would increase to 1395 g/m$^3$. Figure 9 (d) portrays the trend of TDS changes under climate-change conditions in the autumn. It is seen the TDS reach 1365 g/m$^3$ with depth. TDS stratification is more pronounced with decreasing depth.

Generally, Fig. 9 shows that in the spring, as the temperature increases, the surface temperature of the water increases as well, and the extreme thermal gradient will occur near the surface of the water. The intensity of the sun's radiation is not too high to penetrate the depths, and in addition, the inability of the wind to move the layers does not cause epilimnion to form. Also, Fig. 9 shows that as the temperature increases in summer, the surface water temperature rises. In this season, solar radiation is more intense and penetrates deeper. A severe thermal gradient is created. This gradient is from 10 to 27 °C, which causes severe changes in concentration. Therefore, TDS is diluted near the reservoir water surface and its concentration decreases. The thermal gradient would be more severe than in the corresponding period of the baseline period, while the reservoir inflow decreases due to increased temperature.

Evaporation from the water surface increases. These factors would significantly affect the TDS concentration. The water surface temperature would decrease and approach the temperature of the lower layers as the temperature decreases in the autumn. Temperature variations in the reservoir range from 9 to 11 °C. The reservoir inflow would have higher TDS and the TDS concentration at lower reservoir depth would increase.

### 3.4 TDS Gradient near Aidoghmoush Dam under Climate-Change Conditions

Figure 10 depicts the depth profile of TDS in the vicinity of the dam under climate-change conditions relative to the baseline period for (a) the beginning, (b) the middle, and (c) the end of the simulation season in winter; for (d) the beginning, (e) the middle, and (f) the end of the simulation period in the spring; for (g) the beginning,

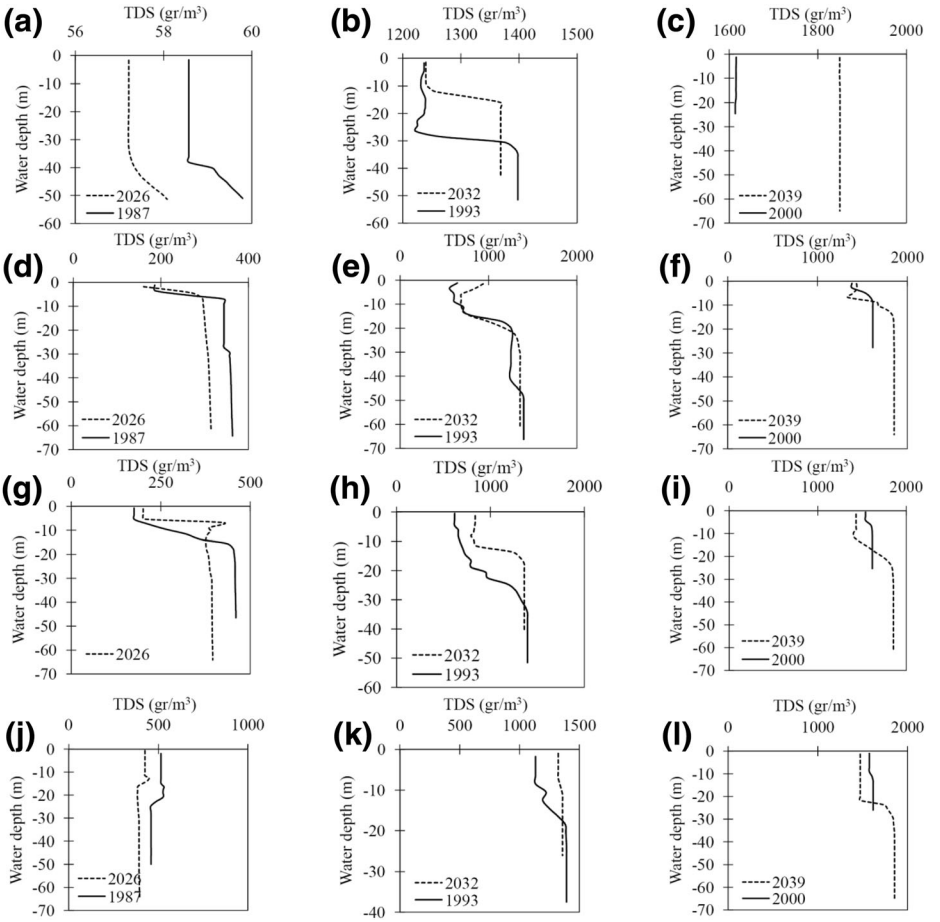


**Fig. 10** Comparison of the depth profile of TDS in the vicinity of the dam under climate-change conditions relative to the baseline period for (a) the beginning, (b) the middle, and (c) the end of the simulation season in winter; for (d) the beginning, (e) the middle, and (f) the end of the simulation period in the spring; for (g) the beginning, (h) the middle, and (i) the end of the simulation season in summer; and for (j) the beginning, (k) the middle and (l) the end of the simulation season in the autumn

(h) the middle, and (i) the end of the simulation season in summer; and for (j) the beginning, (k) the middle and (l) the end of the simulation season in the autumn. The beginning years, middle years, and end years corresponding to baseline and a climate-change conditions are (1987, 2026), (1993, 2032), and (2000, 2039) respectively.

It is seen in Figs. 10 (a) that at the beginning of the simulation period (1987 for the base period and 2026 for the climate change period) in the winter the TDS under climate change would be lower than during the baseline period, but the trends of TDS with depth under baseline and climate-change conditions are similar. The TDS at 30 to 40 m beneath the water surface are uniform, and from there increase with increasing depth. The TDS gradient becomes more pronounced relative to the beginning of the simulation periods in the middle of the simulation periods [Fig. 10 (b)] (1993 under baseline conditions and 2032 under climate-change conditions). TDS would be less in the Epilimnion and Metalimnion than in the Hypolimnion. There are pronounced changes in TDS at shallow depth under climate change conditions (year 2032) relative to the baseline conditions (year 1993) because the Metalimnion increases its depth relative to the baseline condition. The TDS profile would be relatively uniform with depth at the end of the simulation (2000 baseline period, 2039 climate-change conditions). Figures 10 (d) to (f) shows the comparison of TDS depth profiles in spring at the beginning, the middle, and the end of the simulations for the baseline and climate-change periods near the Aidoghmoush dam. The concentration of TDS in the Hypolimnion would be lower under climate-change conditions at the beginning of the simulation period [Fig. 10 (d)] (1987 for base conditions and 2026 for climate change conditions) than during the baseline period. The Epilimnion vanishes and the thickness of the Metalimnion would also be very narrow. The Metalimnion would be near the water surface. The range of TDS change in the middle of the simulation period [Fig. 10 (e)] under climate-change period (2032) would be larger than during the baseline base period (1993). The trends of TDS changes are approximately equal for both periods. There are pronounced changes of TDS near the water surface (about 10–20 m thick region) at the end of the simulation period [Fig. 9(f)]. The TDS changes under climate-change conditions (2039) would exceed the changes during baseline conditions (2000). Figures 10 (g) through (i) show the changes of TDS in the reservoir in the summer under climate-change and baseline periods at the beginning, middle, and end of each simulation period. The TDS in the Epilimnion and Metalimnion at the beginning of the simulation periods [Fig. 10 (g)] under climate-change conditions (2026) exceed the TDS under the baseline condition. The region over which TDS changes occur in the Metalimnion is larger during the baseline period than under climate-change conditions. The gradient of TDS increases near the water surface in the middle of the simulation periods [Fig. 10 (h)]. The TDS decrease near the surface and increases with depth (temperature decreases with increasing depth). The TDS under climate change conditions (2032) would be higher than under baseline conditions (1993). The TDS in the reservoir would increase relative to the beginning and the middle of the simulation periods at the end of the simulation periods [Fig. 10 (i)]. The Metalimnion thickness would be larger under climate-change conditions (2039) than under baseline conditions (2000). The TDS would be higher under baseline conditions than under climate-change condition. Figs. 10 (j) to (l) show changes in TDS with reservoir depth in the autumn under baseline and climate-change conditions at the beginning, middle, and the end of the

simulation periods. The patterns of TDS are different from those of the other three seasons. TDS would be lower under climate-change conditions (2026) than during the baseline period (1987). The TDS would be larger in mid autumn under climate-change conditions (2032) than under baseline conditions (1993). The thickness of the Metalimnion would be very narrow, and the change of TDS in this region would be small. The change in TDS concentration at the end of the simulation period (2039) under climate-change conditions in the Metalimnion would exceed the changes simulated under baseline conditions. The Metalimnion layer would be very narrow under baseline conditions. The TDS under climate-change conditions of in the Epilimnion and Metalimnion would be less than under baseline conditions, and TDS increase with increasing depth.

Figure 10 shows that in winter the decrease of temperature, the change in the angle of sunshine, and the shortening of the length of the days as well as the increase in the cloud cover, affect the temperature of the reservoir water. In some years, the layering is reversed, and in some cases complete mixing is formed and, in some years, too thin stratification is formed in the reservoir. Changes in temperature modify the TDS. A thermal gradient would occur near the water surface in spring as temperature rises, and there is no complete stratification or epilimnion. This is due to the lack of high wind speed that would shift layers, and to low light intensity that does not to penetrate deeper layers. These processes affect concentration changes and cause TDS to dilute near the water surface, resulting in lower concentrations in those areas. These conditions change in summer with increasing air temperature, increasing the length of the day and sunlight, and creating thermal stratification. The Metalimnion prevents the flows of heat and oxygen to the Hypolimnion, where the concentration of TDS increases, and the presence of anaerobic conditions worsen the water quality of the reservoir. In such a situation, water withdrawal from different layers causes layers to mix and improve their water quality. The air temperature in the Autumn is reduced and the water-surface temperature approaches the temperature of the lower layers producing mixing. Therefore, the depth of the epilimnion would increase and the water near the surface would be less concentrated. Wind speed would displace the water layers. Consequently, Metalimnion and pronounced changes in TDS would occur at lower level beneath the water surface. Therefore, factors such as air temperature, water temperature, cloud cover, sunlight, wind speed, time of the day, and changes in reservoir inflow and outflow affect water temperature and TDS in the reservoir.

### 3.5 Variation of TDS along the Reservoir at Average Depth

Figures 11 and 12 display the TDS at average depth in the Aidoghmoush reservoir in mid summer, mid autumn, mid winter, and mid spring, corresponding to baseline (Fig. 11) and climate-change (Fig. 12) conditions. The TDS at the average water depth are low near the entrance of the reservoir and increases with decreasing distance from the dam, in general. Figures 11 (a) and 12 (a) show that TDS concentration in mid summer under climate-change conditions is lower than under baseline conditions in most of the reservoir, which is due to increased air temperature and changes in reservoir inflow under climate-change conditions. The same pattern of TDS is evident in the other seasons. It is seen in Figs. 11 (b) and 12 (b) that under conditions of climate change the areas with maximum and minimum TDS are very similar during the autumn to those in the summer. During the autumn the area with low TDS is wider at the average depth of water than in the other seasons. Figures 11 (c) and (Lee et al.,

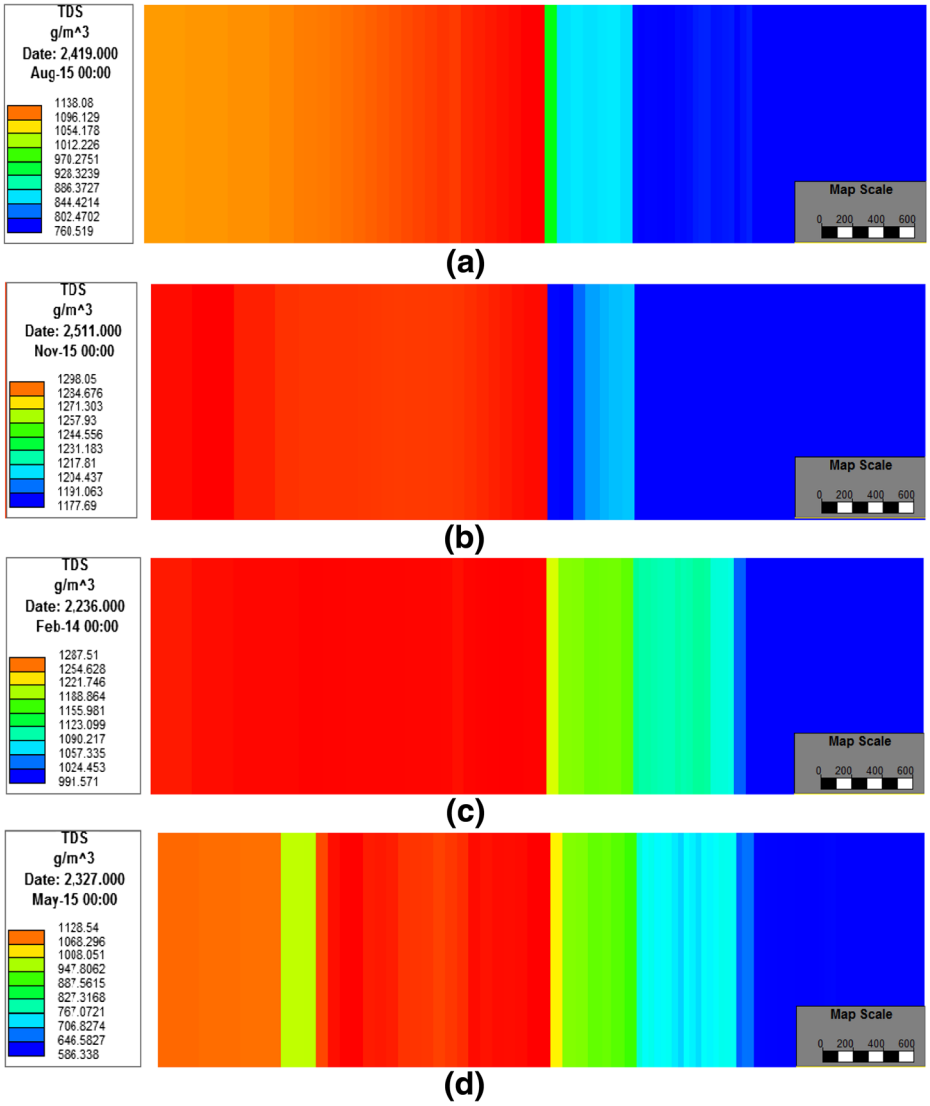


**Fig. 11** TDS variation along average reservoir depth under baseline conditions, in mid summer (a); autumn (b); winter (c); and spring (d) (Baseline conditions correspond to 1993). (The horizontal view is based on 81 sections and it is parallel to the length of the lake measured from the entrance of river flow to the reservoir (right side) to crown of the dam (left side), and the vertical view is parallel to the width of Reservoir Lake and it is the width of section)

2012) (c) show TDS in mid winter under baseline and climate-change conditions, respectively. TDS are high in the reservoir over a wide area. This trend intensifies in the spring season. Figure 11 (d) and (Lee et al., 2012) (d) show that TDS conditions are worst (highest concentration) in mid spring at the average water depth. Therefore, water withdrawal from the average water depth would not be appropriate in the spring. Figures 11 and 12 display the areas with high and low concentrations are similar under climate-change and baseline periods, and TDS are high over a large area of the reservoir.

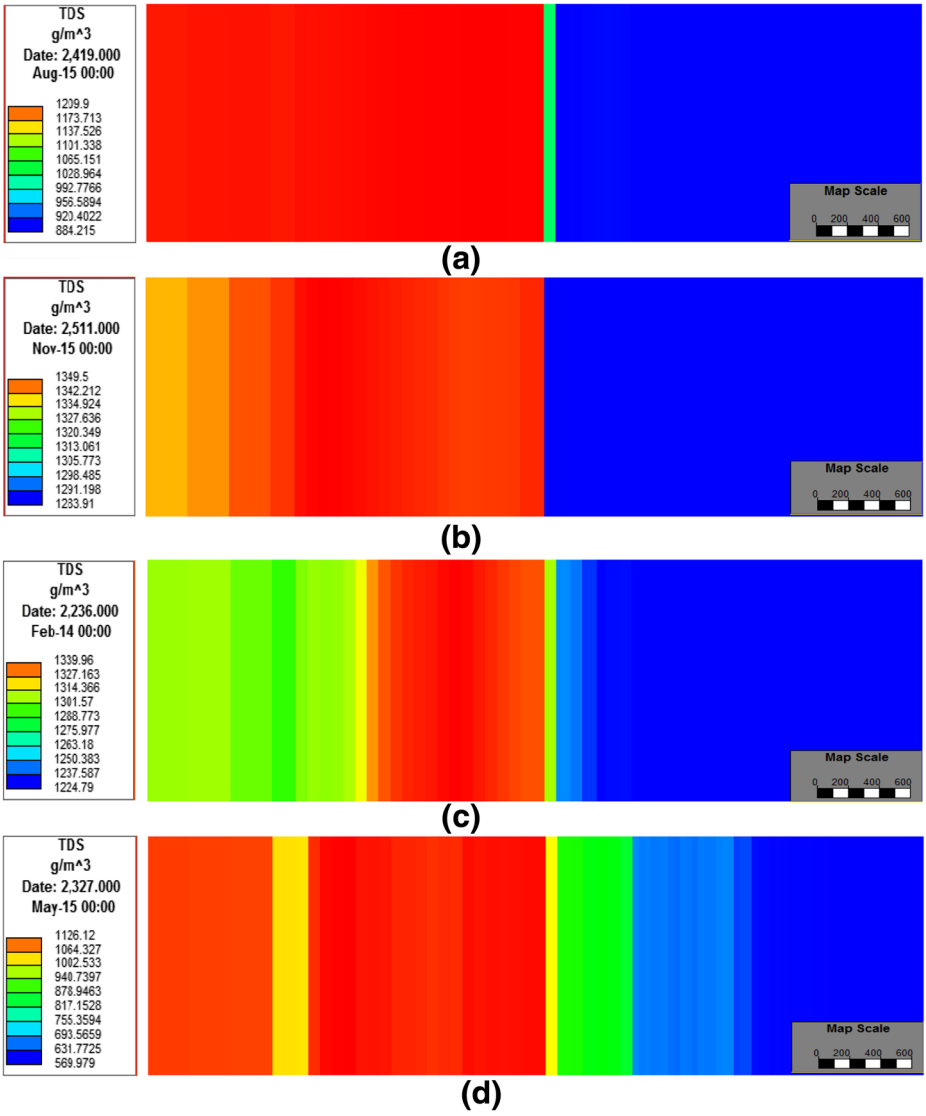


**Fig. 12** TDS variation along average reservoir depth under climate change conditions, in mid summer (a); autumn (b); winter (c); and spring (d) (climate-change conditions correspond to 2032) (The horizontal view is based on 81 sections and it is parallel to the length of the lake measured from the entrance of river flow into the reservoir (right side) to crown of the dam (left side), and the vertical view is parallel to the width of Reservoir Lake and it is the width of section)

## 4 Concluding Remarks

This study has projected the effects of climate change on reservoir TDS and water temperature for future conditions in the Aidoghmoush reservoir (East Azerbaijan-Iran). The results show that under climate-change conditions the air temperature would rise by an average of 1.3 °C relative to the baseline conditions. Also, the reservoir surface-water and bottom-water temperatures would increase by 1.19 and 1.24 °C, respectively. The Aidoghmoush Reservoir Lake

is a type of Warm-Monomictic Lake where there is complete mixing during the winter season and thermal stratification in the other seasons. This paper projects the average TDS concentration at the water surface would be higher under future conditions than under baseline conditions by 44.5 g/m$^3$ (4.3%). Changes in TDS concentration and temperature are correlated, and in areas with intense thermal gradient there are significant changes in TDS. These paper's results indicate differences in the magnitude and timing of the maximum and minimum TDS under climate-change conditions relative to the baseline conditions in the Aidoghmoush reservoir. The TDS concentrations at the water surface under baseline and climate-change conditions in every year of the 14-year simulation periods are maximum in the autumn and winter seasons. The minimum TDS for the first 3 years of simulation would occur in the winter (under climate-change conditions), and it would occur in spring and summer under climate-change and baseline conditions for all other simulation years (except in 2033 when the minimum TDS would occur in the autumn). This paper's findings indicate TDS concentration on the bottom of the reservoir is maximum in the winter and autumn under baseline and climate-change conditions (except in 2031 and 2037 under climate-change conditions, and in 1992 under baseline conditions when it would occur during summer). These paper's results can assist in achieving a better understanding of likely changes in TDS in the Aidoghmoush reservoir under climate-change conditions, and to identify the best levels for water withdrawal level thus improving reservoir operation for water-quality purposes under future conditions.

## Compliance with Ethical Standards

**Conflict of Interest** None.

## References

Amirkhani M, Bozorg-Haddad O, Fallah-Mehdipour E, Loáiciga HA (2016) Multiobjective reservoir operation for water quality optimization. J Irrig Drain Eng 142(12). https://doi.org/10.1061/%28ASCE%29IR.1943-4774.0001105

Ashofteh P-S, Bozorg-Haddad O, Mariño MA (2013) Scenario assessment of streamflow simulation and its transition probability in future periods under climate change. Water Resour Manag 27(1):255–274. https://doi.org/10.1007/s11269-012-0182-2

Ashofteh P-S, Bozorg-Haddad O, Loáiciga HA (2017a) Development of adaptive strategies for irrigation water demand management under climate change. J Irrig Drain Eng 143(2). https://doi.org/10.1061/(ASCE)IR.1943-4774.0001123

Ashofteh P-S, Bozorg-Haddad O, Loáiciga HA (2017b) Logical genetic programming (LGP) development for irrigation water supply hedging under climate-change conditions. Irrig Drain 66(4):530–541. https://doi.org/10.1002/ird.2144

Butcher JB, Nover D, Johnson TE, Clark CM (2015) Sensitivity of lake thermal and mixing dynamics to climate change. Clim Chang 129(1–2):295–305. https://doi.org/10.1007/s10584-015-1326-1

Chung SW, Gu RR (2009) Prediction of the fate and transport processes of atrazine in a reservoir. Environ Manag 44(1):46–61. https://doi.org/10.1007/s00267-009-9312-x

Cole, T. M. and S. A. Wells (2006). "CE-QUAL-W2: A two-dimensional, laterally averaged, Hydrodynamic and Water Quality Model, Version 3.5," Instruction Report EL-06-1, US Army Engineering and Research Development Center, Vicksburg, Ms

Debele B, Srinivasan R, Parlange J-Y (2008) Coupling upland watershed and downstream waterbody hydrodynamic and water quality models (SWAT and CE-QUAL-W2) for better water resources management in complex river basins. Environ Model Assess 13(1):135–153. https://doi.org/10.1007/s10666-006-9075-1

Heidarzadeh and Motiey Nejad (2017) simulated the TDS by CE-QUAL-W2 in two scenarios of with and without sedimentation in normal, dry, and wet periods of inflow for Shahriyar reservoir, Iran. With the

outflow TDS, there was no limitation to use of reservoir water for agricultural purposes based on FAO irrigation guidelines for both scenarios

IPCC-TGCIA (Intergovernmental Panel on Climate Change, Task Group on Scenarios for Climate Impact Assessment). (1999). Guideline on the use of scenario date for climate impact and adaptation assessment. Version 1, T .R. Carter, M. Hullme, and M. Lal, eds., Intergovernmental Panel on Climate Change, Task Group on Scenarios for Climate Impact Assessment,69

IPCC-DDC. (1988). "Data distribution center." < http: / ipcc-ddccru.uea.ac.uk/ >

Lee HW, Kim EJ, Park SS, Choi JH (2012) Effects of climate change on the thermal structure of lakes in the asian monsoon area. Clim Chang 112(3–4):859–880. https://doi.org/10.1007/s10584-011-0233-3

Liu W-C, Chen W-B, Kimura N (2009) Impact of phosphorus load reduction on water quality in a stratified reservoir-eutrophication modeling study. Environ Monit Assess 159(1–4):393–406. https://doi.org/10.1007/s10661-008-0637-3

Liu WC, Chen WB (2013) Modeling hydrothermal, suspended solids transport and residence time in a deep reservoir. Int J Environ Sci Technol 10(2):251–260. https://doi.org/10.1007/s13762-012-0147-2

Peng H, Zheng X, Chen L, Wei Y (2016) Analysis of numerical simulation and influencing factors of seasonal manganese pollution in reservoirs. Environ Sci Pollut Res 23(14):14362–14372. https://doi.org/10.1007/s11356-016-6380-3

Sabeti, R., Jamali, S., and Hajikandi-Jamali, H. (2017) "Simulation of thermal stratification and salinity using the Ce-Qual-W2 model (case study: mamloo dam)". Engineering, Technology & Applied Science Research, 1664–1669

Shokri A, Bozorg-Haddad O, Mariño MA (2014) Multi-objective quantity–quality reservoir operation in sudden pollution. Water Resour Manag 28(2):567–586

Soleimani S, Bozorg-Haddad O, Saadatpour M, Loáiciga HA (2016) Optimal selective withdrawal rules using a coupled data mining model and genetic algorithm. J Water Resour Plan Manag 142(12). https://doi.org/10.1061/%28ASCE%29WR.1943-5452.0000717

Vaighan AA, Talebbeydokhti N, Massah Bavani A (2017) Assessing the impacts of climate and land use change on streamflow, water quality and suspended sediment in the Kor River basin, southwest of Iran. Environ Earth Sci 76:543. https://doi.org/10.1007/s12665-017-6880-6

Yazdi J, Moridi A (2017) Interactive reservoir-watershed modeling framework for integrated water quality management. Water Resour Manag 31(7):2105–2125. https://doi.org/10.1007/s11269-017-1627-4

## Affiliations

**Firoozeh Azadi[1] · Parisa-Sadat Ashofteh[1] · Hugo A. Loáiciga[2]**

Firoozeh Azadi
f.azadi@stu.qom.ac.ir

Hugo A. Loáiciga
Hugo.Loaiciga@geog.ucsb.edu; hugo@geog.ucsb.edu; hloaiciga@ucsb.edu

[1] Department of Civil Engineering, University of Qom, Qom, Iran

[2] Department of Geography, University of California, Santa Barbara, CA 93016-4060, USA